Advances in Military Technology
Vol. 20, No. 2, 2025, pp. 601-619
ISSN 1802-2308, eISSN 2533-4123
DOI 10.3849/aimt.02031

Investigation of Vehicle Vibrations During Traversal of Speed Bumps

B. Viet Dung*, M. Macko, and D. Ba Ngoc

Department of Weapons and Ammunition, University of Defence, Brno, Czech Republic

The manuscript was received on 28 August 2025 and was accepted
after revision for publication as an original research paper on 15 December 2025.

Abstract:

Speed bumps are commonly used to reduce accidents caused by excessive speed, especially in populated or narrow areas. Their design and placement, however, must ensure vehicle stability and driver comfort. This study develops an 8-degree-of-freedom (8-DoF) vehicle vibration model incorporating road surface equations with various speed bump configurations. Different bump heights and staggered arrangements are analyzed to produce complex vibration responses. Experimental tests on a 2019 Toyota RAV4 validate the model by measuring vibrations over multiple bump types. The results show strong agreement between simulated and experimental data, offering valuable guidance for designing speed bumps that effectively enhance traffic safety while minimizing discomfort.

Keywords:

vehicle dynamics, speed bumps, vibration analysis, suspension system, ride comfort

Introduction

Speed bumps are typically installed on road sections with high traffic density, near entrances and exits, pedestrian crossings, or hazardous areas such as downhill slopes or sharp curves. The primary purpose of installing speed bumps is to compel vehicles to reduce their speed, thereby lowering the risk of accidents and enhancing safety for both pedestrians and other road users. In addition, speed bumps help regulate vehicle speeds within designated limits, while allowing the suspension system to effectively absorb vibrations, thereby improving ride comfort and vehicle stability on uneven surfaces. Studying how vehicles traverse different types of speed bumps, such as trapezoidal, half-sine, and rectangular shapes, provides a scientific basis for their optimal

* *Corresponding author: Department of Weapons and Ammunition, University of Defence, Kounicova 156/65, CZ-662 10 Brno, Czech Republic. Phone: +420 774 097 452, E-mail: vietdung.bui@unob.cz. ORCID 0009-0004-9752-9054.*

placement in various areas and speed-limit zones, thus enhancing both comfort and safety during operation.

The study [1] investigates the optimization of vehicle speed when passing over different types of speed bumps to enhance both comfort and safety. Using a 4-degree-of-freedom suspension model and simulating vehicle vibrations on sinusoidal, rectangular, and trapezoidal speed bumps, the study applies an immune algorithm to determine the optimal speed. Results show that this method significantly reduces vibrations, acceleration, suspension deflection, and tire load, achieving a balance between comfort and safety. Additionally, the paper identifies the comfortable speed ranges for each type of speed bump, providing a scientific basis for designing and placing speed bumps in accordance with speed limits and varying road conditions.

In [2], the vertical vibration of a two-axle vehicle when traversing transverse speed bumps is investigated. The analysis employs quarter-, half-, and full-vehicle models, with the full model best capturing the vehicle's geometric and structural asymmetry. Both symmetric and asymmetric excitations are considered, and Heaviside's function is applied to model vibration inputs. Experiments were conducted on a Tr 21 trolleybus using standardized speed bumps, measuring vertical displacements, velocities, and accelerations of the axles and vehicle body, including under the driver's seat. These vibrations significantly affect driver comfort, fatigue, and health. Proper selection of a spatial vehicle model is essential for both experimental and theoretical studies of vertical vibrations.

According to [3], speed management is a method to reduce the adverse effects of overspeeding, with speed control undulations (SCUs) being a key tool in urban areas. The study evaluated narrow (bump) and wide (hump) SCUs with heights of 5 cm and 10 cm regarding discomfort for drivers and passengers. Whole-body vibration (WBV) was recorded in passenger cars at speeds of 20, 30, 40, and 50 km/h and analyzed in accordance with ISO 2631-1. The vibration data were analyzed using a_w (average weighted acceleration) and the MTVV parameter (maximum transient vibration value). The results indicate that humps generate lower vibration levels than bumps of the same height. Previous studies also confirm that humps are healthier and more comfortable. SCU design and geometry significantly affect vibration and comfort. Some studies suggest optimizing SCU cross-sections to reduce adverse effects. SCUs are considered economical and effective for reducing speed, accidents, and improving traffic safety.

The study [4] develops a full-vehicle 8-DoF model with an active suspension system and designs a fuzzy-PID controller, which significantly improves ride comfort and driving stability. Continuous speed bump profiles and C-level road surfaces are used as inputs for vibration analysis. The results show that the fuzzy-PID suspension system considerably reduces vertical, pitch, and roll vibrations of the vehicle body, while also improving suspension dynamic deflection and tire dynamic load.

In this study, a detailed mathematical model of an 8-degree-of-freedom (8-DoF) vehicle with an independent suspension system is developed, incorporating speed bumps of bar, semi-sine, and rectangular shapes. The model is simulated in Matlab/Simulink under constant vehicle speed to compare the resulting vibration responses. Experimental tests are conducted on a 2019 Toyota RAV4 passing over speed bumps of varying widths. Vehicle vibrations are measured using iDynamics software installed on a smartphone, providing three-dimensional acceleration data. The experimental results are then compared with theoretical predictions to evaluate model accuracy and analyze the factors influencing vehicle vibration and ride comfort when traversing speed bumps.

2 Mathematical Model

2.1 System of Mathematical Equations of the Vehicle

The computational model of the vehicle together with the corresponding symbols is illustrated in Fig. 1 [4-7].

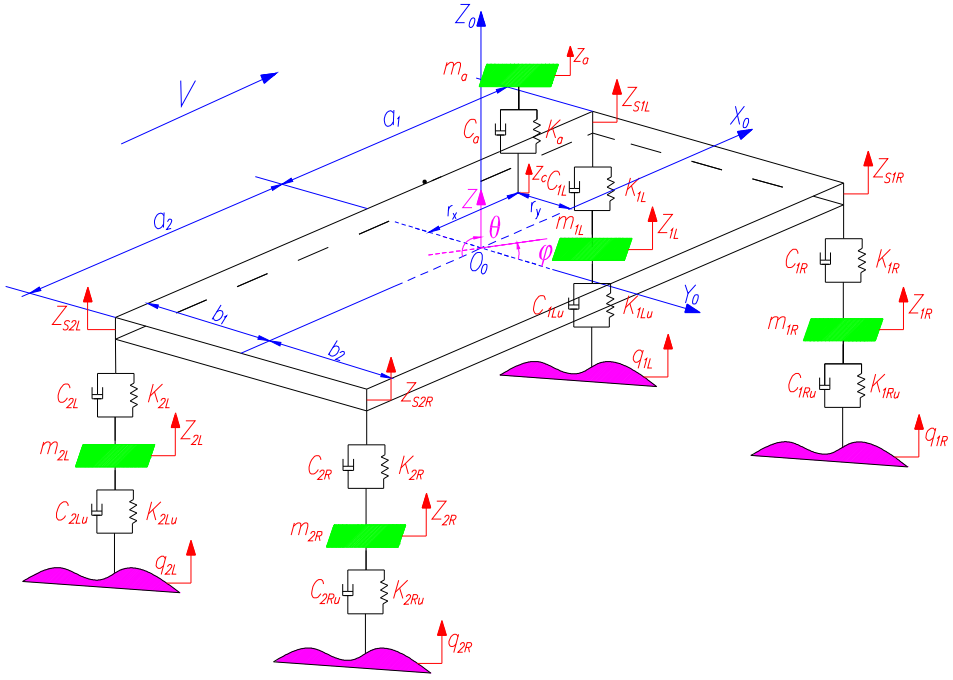

Fig. 1 8-DoF vehicle model

The coordinate system $O_0X_0Y_0Z_0$ is defined at the vehicle center of gravity; q_{1R}, q_{1L}, q_{2R}, q_{2L} – the roughness of the road surface at the contact with the front and rear tires on the right and left; C_{1Ru}, K_{1Ru}, C_{1Lu}, K_{1Lu}, C_{2Ru}, K_{2Ru}, C_{2Lu}, K_{2Lu} – the damping coefficient and elasticity coefficient of the front and rear tires on the right and left; C_{1R}, K_{1R}, C_{1L}, K_{1L}, C_{2R}, K_{2R}, C_{2L}, K_{2L} – the damping coefficient and elasticity coefficient of the front and rear suspension on the right and left; m_{1L}, m_{1R}, m_{2L}, m_{2R} – the unsprung mass; Z_{1L}, Z_{1R}, Z_{2L}, Z_{2R} – the vertical displacements of the unsprung mass; Z_{S1L}, Z_{S1R}, Z_{S2L}, Z_{S2R} – the vertical displacements of the sprung mass; C_a, K_a – the spring stiffness coefficient and damping coefficient of the human–chair system; m_a, Z_a – the mass and vertical displacement of the human–chair system; Z_c – the vertical displacement at the driver's seat location; Z, θ, φ – the vertical displacement, pitch angle, roll angle of the vehicle; r_x, r_y – the distance from the vehicle's center of gravity to the driver's seat location; a_1, a_2 – the distances from the center of gravity to the front and rear of the vehicle; b_1, b_2 – the distances from the center of gravity to the left and right sides of the vehicle; V – the vehicle speed.

F_{K1Lu}, F_{C1Lu}, F_{K1Ru}, F_{C1Ru}, F_{K2Lu}, F_{C2Lu}, F_{K2Ru}, F_{C2Ru} – the elastic and damping forces at each wheel [4, 6, 8, 9].

$$\begin{aligned} F_{K1Ru} &= K_{1Ru}(Z_{1R} - q_{1R}) & F_{K1Lu} &= K_{1Lu}(Z_{1L} - q_{1L}) \\ F_{C1Ru} &= C_{1Ru}(Z'_{1R} - q'_{1R}) & F_{C1Lu} &= C_{1Lu}(Z'_{1L} - q'_{1L}) \\ F_{K2Ru} &= K_{2Ru}(Z_{2R} - q_{2R}) & F_{K2Lu} &= K_{2Lu}(Z_{2L} - q_{2L}) \\ F_{C2Ru} &= C_{2Ru}(Z'_{2R} - q'_{2R}) & F_{C2Lu} &= C_{2Lu}(Z'_{2L} - q'_{2L}) \end{aligned} \quad (1)$$

F_{K1L}, F_{C1L}, F_{K1R}, F_{C1R}, F_{K2Lu}, F_{C2L}, F_{K2R}, F_{C2R} – the elastic and damping forces in the suspension systems [8, 9].

$$\begin{aligned} F_{K1R} &= K_{1R}(Z_{S1R} - Z_{1R}) & F_{K1L} &= K_{1L}(Z_{S1L} - Z_{1L}) \\ F_{C1R} &= C_{1R}(Z'_{S1R} - Z'_{1R}) & F_{C1L} &= C_{1L}(Z'_{S1L} - Z'_{1L}) \\ F_{K2R} &= K_{2R}(Z_{S2R} - Z_{2R}) & F_{K2L} &= K_{2L}(Z_{S2L} - Z_{2L}) \\ F_{C2R} &= C_{2R}(Z'_{S2R} - Z'_{2R}) & F_{C2L} &= C_{2L}(Z'_{S2L} - Z'_{2L}) \end{aligned} \quad (2)$$

F_{Ka}, F_{Ca} – the elastic and damping forces of the human-chair system [4].

$$\begin{aligned} F_{Ka} &= K_a(Z_a - Z_c) \\ F_{Ca} &= C_a(Z'_a - Z'_c) \end{aligned} \quad (3)$$

Express the variables Z_{S1L}, Z_{S1R}, Z_{S2L}, Z_{S2R}, Z_c in terms of the variables Z, θ, φ as follows [4, 6]:

$$\begin{aligned} Z_{S1L} &= Z - a_1\theta - b_1\varphi \\ Z_{S2L} &= Z + a_2\theta - b_1\varphi \\ Z_{S1R} &= Z - a_1\theta + b_2\varphi \\ Z_{S2R} &= Z + a_2\theta + b_2\varphi \\ Z_c &= Z - r_x\theta - r_y\varphi \end{aligned} \quad (4)$$

Substitute expressions (4) into (2) and (3):

$$\begin{cases} F_{K1R} = K_{1R}(Z - a_1\theta + b_2\varphi - Z_{1R}) \\ F_{C1R} = C_{1R}(Z' - a_1\theta' + b_2\varphi' - Z'_{1R}) \\ F_{K2R} = K_{2R}(Z + a_2\theta + b_2\varphi - Z_{2R}) \\ F_{C2R} = C_{2R}(Z' + a_2\theta' + b_2\varphi' - Z'_{2R}) \end{cases}$$

$$\begin{cases} F_{K1L} = K_{1L}(Z - a_1\theta - b_1\varphi - Z_{1L}) \\ F_{C1L} = C_{1L}(Z' - a_1\theta' - b_1\varphi' - Z'_{1L}) \\ F_{K2L} = K_{2L}(Z + a_2\theta - b_1\varphi - Z_{2L}) \\ F_{C2L} = C_{2L}(Z' + a_2\theta' - b_1\varphi' - Z'_{2L}) \end{cases} \quad (5)$$

$$\begin{cases} F_{Ka} = K_a(Z_a - Z + r_x\theta + r_y\varphi) \\ F_{Ca} = C_a(C'_a - Z' + r_x\theta' + r_y\varphi') \end{cases}$$

The system of differential equations describing the vibrations of the 8-DoF vehicle consists of 8 equations with 8 unknowns Z_{1L}, Z_{1R}, Z_{2L}, Z_{2R}, Z_a, Z, θ, φ:

$$
\begin{aligned}
m_{1R}Z''_{1R} &= F_{K1R} + F_{C1R} - F_{K1Ru} - F_{C1Ru} \\
m_{2R}Z''_{2R} &= F_{K2R} + F_{C2R} - F_{K2Ru} - F_{C2Ru} \\
m_{1L}Z''_{1L} &= F_{K1L} + F_{C1L} - F_{K1Lu} - F_{C1Lu} \\
m_{2L}Z''_{2L} &= F_{K2L} + F_{C2L} - F_{K2Lu} - F_{C2Lu} \\
m_aZ''_a &= -F_{Ka} - F_{Ca} \\
MZ'' &= -F_{K1R} - F_{C1R} - F_{K2R} - F_{C2R} - F_{K1L} - F_{C1L} - F_{K2L} - F_{C2L} + F_{Ka} + F_{Ca} \\
J_y\theta'' &= a_1(F_{K1R} + F_{C1R} + F_{K1L} + F_{C1L}) - a_2(F_{K2R} + F_{C2R} + F_{K2L} + F_{C2L}) - \\
&\quad - r_x(F_{Ka} + F_{Ca}) \\
J_x\varphi'' &= b_1(F_{K1L} + F_{C1L} + F_{K2L} + F_{C2L}) - b_2(F_{K1R} + F_{C1R} + F_{K2R} + F_{C2R}) - \\
&\quad - r_y(F_{Ka} + F_{Ca})
\end{aligned}
\tag{6}
$$

2.2 The Mathematical Equations of Rough Road Profiles

This study investigates road surface profile models, including trapezoidal, semi-sinusoidal, and rectangular shapes in Figs 2-4. The left speed bump has a height of 0.1 m, while the right one is 0.15 m, both with a width of 2 m. The speed bumps are arranged in an offset configuration. The vehicle travels at a constant speed of V = 8.33 m/s. The mathematical model of rough road profiles is as follows [1, 6]:

- trapezoidal speed bump

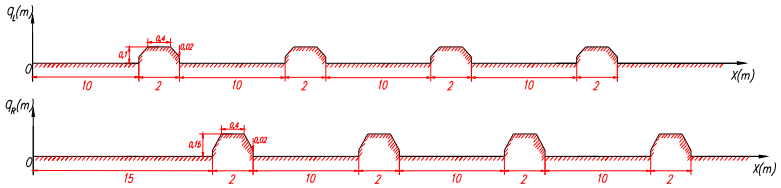

Fig. 2 Trapezoidal speed bump profile

Eq. (7):

$$q_{1L}=\begin{cases}0 & (0\le t<1.2\text{ s})\\ 0.02 & (t=1.2\text{ s})\\ \frac{5t}{6}-0.98 & (1.2\text{ s}<t<1.296\text{ s})\\ 0.1 & (1.296\text{ s}\le t\le 1.344\text{ s})\\ -\frac{5t}{6}+1.22 & (1.344\text{ s}<t<1.44\text{ s})\\ 0.02 & (t=1.44\text{ s})\\ 0 & (1.44\text{ s}<t<2.64\text{ s})\\ 0.02 & (t=2.64\text{ s})\\ \frac{5t}{6}-2.18 & (2.64\text{ s}<t<2.736\text{ s})\\ 0.1 & (2.736\text{ s}\le t\le 2.784\text{ s})\\ -\frac{5t}{6}+2.42 & (2.784\text{ s}<t<2.88\text{ s})\\ 0.02 & (t=2.88\text{ s})\\ 0 & (2.88\text{ s}<t<4.08\text{ s})\\ 0.02 & (t=4.08\text{ s})\\ \frac{5t}{6}-3.38 & (4.08\text{ s}<t<4.176\text{ s})\\ 0.1 & (4.176\text{ s}\le t\le 4.224\text{ s})\\ -\frac{5t}{6}+3.62 & (4.224\text{ s}<t<4.32\text{ s})\\ 0.02 & (t=4.32\text{ s})\\ 0 & (4.32\text{ s}<t<5.52\text{ s})\\ 0.02 & (t=5.52\text{ s})\\ \frac{5t}{6}-4.58 & (5.52\text{ s}<t<5.616\text{ s})\\ 0.1 & (5.616\text{ s}\le t\le 5.664\text{ s})\\ -\frac{5t}{6}+4.82 & (5.664\text{ s}<t<5.76\text{ s})\\ 0.02 & (t=5.76\text{ s})\\ 0 & (t>5.76\text{ s})\end{cases}$$

$$q_{1R}=\begin{cases}0 & (0\le t<1.8\text{ s})\\ 0.02 & (t=1.8\text{ s})\\ \frac{65t}{48}-2.4175 & (1.8\text{ s}<t<1.896\text{ s})\\ 0.15 & (1.896\text{ s}\le t\le 1.944\text{ s})\\ -\frac{65t}{48}+2.7825 & (1.944\text{ s}<t<2.04\text{ s})\\ 0.02 & (t=2.04\text{ s})\\ 0 & (2.04\text{ s}<t<3.24\text{ s})\\ 0.02 & (t=3.24\text{ s})\\ \frac{65t}{48}-4.3675 & (3.24\text{ s}<t<3.336\text{ s})\\ 0.15 & (3.336\text{ s}\le t\le 3.384\text{ s})\\ -\frac{65t}{48}+4.7325 & (3.384\text{ s}<t<3.48\text{ s})\\ 0.02 & (t=3.48\text{ s})\\ 0 & (3.48\text{ s}<t<4.68\text{ s})\\ 0.02 & (t=4.68\text{ s})\\ \frac{65t}{48}-6.3175 & (4.68\text{ s}<t<4.776\text{ s})\\ 0.15 & (4.776\text{ s}\le t\le 4.824\text{ s})\\ -\frac{65t}{48}+6.6825 & (4.824\text{ s}<t<4.92\text{ s})\\ 0.02 & (t=4.92\text{ s})\\ 0 & (4.92\text{ s}<t<6.12\text{ s})\\ 0.02 & (t=6.12\text{ s})\\ \frac{65t}{48}-8.2675 & (6.12\text{ s}<t<6.216\text{ s})\\ 0.15 & (6.216\text{ s}\le t\le 6.264\text{ s})\\ -\frac{65t}{48}+8.6325 & (6.264\text{ s}<t<6.36\text{ s})\\ 0.02 & (t=6.36\text{ s})\\ 0 & (t>6.36\text{ s})\end{cases}$$

Eq (8):

$$q_{2L}=\begin{cases}0 & (0\le t<1.536\ \text{s})\\ 0.02 & (t=1.536\ \text{s})\\ \frac{5t}{6}-1.26 & (1.536\ \text{s}<t<1.632\ \text{s})\\ 0.1 & (1.632\ \text{s}\le t\le 1.68\ \text{s})\\ -\frac{5t}{6}+1.5 & (1.68\ \text{s}<t<1.776\ \text{s})\\ 0.02 & (t=1.776\ \text{s})\\ 0 & (1.776\ \text{s}<t<2.976\ \text{s})\\ 0.02 & (t=2.976\ \text{s})\\ \frac{5t}{6}-2.46 & (2.976\ \text{s}<t<3.072\ \text{s})\\ 0.1 & (3.072\ \text{s}\le t\le 3.12\ \text{s})\\ -\frac{5t}{6}+2.7 & (3.12\ \text{s}<t<3.216\ \text{s})\\ 0.02 & (t=3.216\ \text{s})\\ 0 & (3.216\ \text{s}<t<4.416\ \text{s})\\ 0.02 & (t=4.416\ \text{s})\\ \frac{5t}{6}-3.66 & (4.416\ \text{s}<t<4.512\ \text{s})\\ 0{,}1 & (4.512\ \text{s}\le t\le 4.56\ \text{s})\\ -\frac{5t}{6}+3.9 & (4.56\ \text{s}<t<4.656\ \text{s})\\ 0.02 & (t=4.656\ \text{s})\\ 0 & (4.656\ \text{s}<t<5.856\ \text{s})\\ 0.02 & (t=5.856\ \text{s})\\ \frac{5t}{6}-4.86 & (5.856\ \text{s}<t<5.952\ \text{s})\\ 0.1 & (5.952\ \text{s}\le t\le 6\ \text{s})\\ -\frac{5t}{6}+5.1 & (6\ \text{s}<t<6.096\ \text{s})\\ 0.02 & (t=6.096\ \text{s})\\ 0 & (t>6.096\ \text{s})\end{cases}, q_{2R}=\begin{cases}0 & (0\le t<2.136\ \text{s})\\ 0.02 & (t=2.136\ \text{s})\\ \frac{65t}{48}-2.8725 & (2.136\ \text{s}<t<2.232\ \text{s})\\ 0.15 & (2.232\ \text{s}\le t\le 2.28\ \text{s})\\ -\frac{65t}{48}+3.2375 & (2.28\ \text{s}<t<2.376\ \text{s})\\ 0.02 & (t=2.376\ \text{s})\\ 0 & (2.376\ \text{s}<t<3.576\ \text{s})\\ 0.02 & (t=3.576\ \text{s})\\ \frac{65t}{48}-4.8225 & (3.576\ \text{s}<t<3.672\ \text{s})\\ 0.15 & (3.672\ \text{s}\le t\le 3.72\ \text{s})\\ -\frac{65t}{48}+5.1875 & (3.72\ \text{s}<t<3.816\ \text{s})\\ 0.02 & (t=3.816\ \text{s})\\ 0 & (3.816\ \text{s}<t<5.016\ \text{s})\\ 0.02 & (t=5.016\ \text{s})\\ \frac{65t}{48}-6.7725 & (5.016\ \text{s}<t<5.112\ \text{s})\\ 0.15 & (5.112\ \text{s}\le t\le 5.16\ \text{s})\\ -\frac{65t}{48}+7.1375 & (5.16\ \text{s}<t<5.256\ \text{s})\\ 0.02 & (t=5.256\ \text{s})\\ 0 & (5.256\ \text{s}<t<6.456\ \text{s})\\ 0.02 & (t=6.456\ \text{s})\\ \frac{65t}{48}-8.7225 & (6.456\ \text{s}<t<6.552\ \text{s})\\ 0.15 & (6.552\ \text{s}\le t\le 6.6\ \text{s})\\ -\frac{65t}{48}+9.0875 & (6.6\ \text{s}<t<6.696\ \text{s})\\ 0.02 & (t=6.696\ \text{s})\\ 0 & (t>6.696\ \text{s})\end{cases}$$

- semi-sinusoidal speed bump,

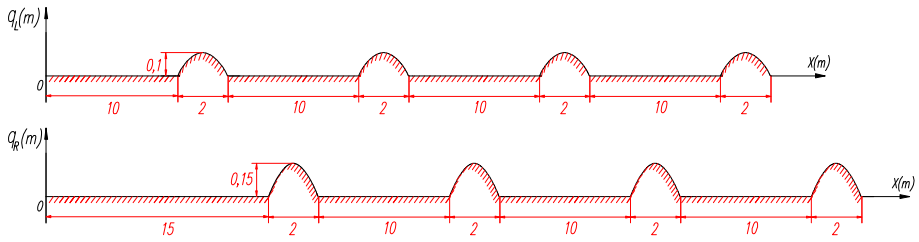

Fig. 3 Semi-sinusoidal speed bump profile

$$q_{1L} = \begin{cases} 0 \quad (0 \le t < 1.2 \text{ s}) \\ 0.1\sin[13.09(t-1.2)] \quad (1.2 \text{ s} \le t < 1.44 \text{ s}) \\ 0 \quad (1.44 \text{ s} \le t < 2.64 \text{ s}) \\ 0.1\sin[13.09(t-2.64)] \quad (2.64 \text{ s} \le t < 2.88 \text{ s}) \\ 0 \quad (2.88 \text{ s} \le t < 4.08 \text{ s}) \\ 0.1\sin[13.09(t-4.08)] \quad (4.08 \text{ s} \le t < 4.32 \text{ s}) \\ 0 \quad (4.32 \text{ s} \le t < 5.52 \text{ s}) \\ 0.1\sin[13.09(t-5,52)] \quad (5.52 \text{ s} \le t < 5.76 \text{ s}) \\ 0 \quad (t \ge 5.76 \text{ s}) \end{cases}$$

$$q_{2L} = \begin{cases} 0 \quad (0 \le t < 1.536 \text{ s}) \\ 0.1\sin[13.09(t-1.536)] \quad (1.536 \text{ s} \le t < 1.776 \text{ s}) \\ 0 \quad (1.776 \text{ s} \le t < 2.976 \text{ s}) \\ 0.1\sin[13.09(t-2.976)] \quad (2.976 \text{ s} \le t < 3.216 \text{ s}) \\ 0 \quad (3.216 \text{ s} \le t < 4.416 \text{ s}) \\ 0.1\sin[13.09(t-4.416)] \quad (4.416 \text{ s} \le t < 4.656 \text{ s}) \\ 0 \quad (4.656 \text{ s} \le t < 5.856 \text{ s}) \\ 0.1\sin[13.09(t-5.856)] \quad (5.856 \text{ s} \le t < 6.096 \text{ s}) \\ 0 \quad (t \ge 6.096 \text{ s}) \end{cases} \tag{9}$$

$$q_{1R} = \begin{cases} 0 \quad (0 \le t < 1.8 \text{ s}) \\ 0.15\sin[13.09(t-1.8)] \quad (1.8 \text{ s} \le t < 2.04 \text{ s}) \\ 0 \quad (2.04 \text{ s} \le t < 3.24 \text{ s}) \\ 0.15\sin[13.09(t-3.24)] \quad (3.24 \text{ s} \le t < 3.48 \text{ s}) \\ 0 \quad (3.48 \text{ s} \le t < 4.68 \text{ s}) \\ 0.15\sin[13.09(t-4.68)] \quad (4.68 \text{ s} \le t < 4.92 \text{ s}) \\ 0 \quad (4.92 \text{ s} \le t < 6.12 \text{ s}) \\ 0.15\sin[13.09(t-6.12)] \quad (6.12 \text{ s} \le t < 6.36 \text{ s}) \\ 0 \quad (t \ge 6.36 \text{ s}) \end{cases}$$

$$q_{2R} = \begin{cases} 0 \quad (0 \le t < 2.136 \text{ s}) \\ 0.15\sin[13.09(t-2.136)] \quad (2.136 \text{ s} \le t < 2.376 \text{ s}) \\ 0 \quad (2.376 \text{ s} \le t < 3.576 \text{ s}) \\ 0.15\sin[13.09(t-3.576)] \quad (3.576 \text{ s} \le t < 3.816 \text{ s}) \\ 0 \quad (3.816 \text{ s} \le t < 5.016 \text{ s}) \\ 0.15\sin[13.09(t-5.016)] \quad (5.016 \text{ s} \le t < 5.256 \text{ s}) \\ 0 \quad (5.256 \text{ s} \le t < 6.456 \text{ s}) \\ 0.15\sin[13.09(t-6.456)] \quad (6.456 \text{ s} \le t < 6.696 \text{ s}) \\ 0 \quad (t \ge 6.696 \text{ s}) \end{cases} \tag{10}$$

- rectangular speed bump.

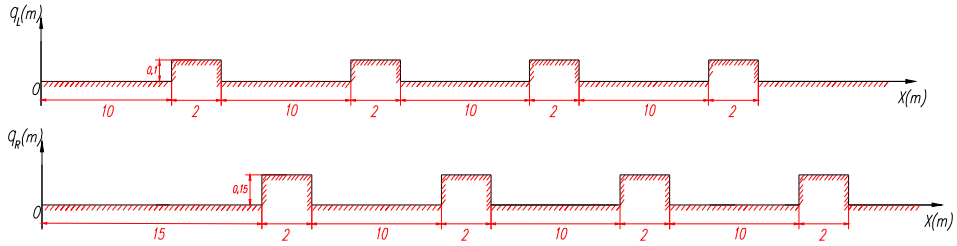

Fig. 4 Rectangular speed bump profile

$$q_{1L} = \begin{cases} 0 & (0 \le t < 1.2\ \text{s}) \\ 0.1 & (1.2\ \text{s} \le t \le 1.44\ \text{s}) \\ 0 & (1.44\ \text{s} < t < 2.64\ \text{s}) \\ 0.1 & (2.64\ \text{s} \le t \le 2.88\ \text{s}) \\ 0 & (2.88\ \text{s} < t < 4.08\ \text{s}) \\ 0.1 & (4.08\ \text{s} \le t \le 4.32\ \text{s}) \\ 0 & (4.32\ \text{s} < t < 5.52\ \text{s}) \\ 0.1 & (5.52\ \text{s} \le t \le 5.76\ \text{s}) \\ 0 & (t > 5.76\ \text{s}) \end{cases}, \quad q_{2L} = \begin{cases} 0 & (0 \le t < 1.536\ \text{s}) \\ 0.1 & (1.536\ \text{s} \le t \le 1.776\ \text{s}) \\ 0 & (1.776\ \text{s} < t < 2.976\ \text{s}) \\ 0.1 & (2.976\ \text{s} \le t \le 3.216\ \text{s}) \\ 0 & (3.216\ \text{s} < t < 4.416\ \text{s}) \\ 0.1 & (4.416\ \text{s} \le t \le 4.656\ \text{s}) \\ 0 & (4.656\ \text{s} < t < 5.856\ \text{s}) \\ 0.1 & (5.856\ \text{s} \le t \le 6.096\ \text{s}) \\ 0 & (t > 6.096\ \text{s}) \end{cases} \tag{11}$$

$$q_{1R} = \begin{cases} 0 & (0 \le t < 1.8\ \text{s}) \\ 0.15 & (1.8\ \text{s} \le t \le 2.04\ \text{s}) \\ 0 & (2.04\ \text{s} < t < 3.24\ \text{s}) \\ 0.15 & (3.24\ \text{s} \le t \le 3.48\ \text{s}) \\ 0 & (3.48\ \text{s} < t < 4.68\ \text{s}) \\ 0.15 & (4.68\ \text{s} \le t \le 4.92\ \text{s}) \\ 0 & (4,92\ \text{s} < t < 6.12\ \text{s}) \\ 0.15 & (6.12\ \text{s} \le t \le 6.36\ \text{s}) \\ 0 & (t > 6.36\ \text{s}) \end{cases}, \quad q_{2R} = \begin{cases} 0 & (0 \le t < 2.136\ \text{s}) \\ 0.15 & (2.136\ \text{s} \le t \le 2.376\ \text{s}) \\ 0 & (2.376\ \text{s} < t < 3.576\ \text{s}) \\ 0.15 & (3.576\ \text{s} \le t \le 3.816\ \text{s}) \\ 0 & (3.816\ \text{s} < t < 5.016\ \text{s}) \\ 0.15 & (5.016\ \text{s} \le t \le 5.256\ \text{s}) \\ 0 & (5.256\ \text{s} < t < 6.456\ \text{s}) \\ 0.15 & (6.456\ \text{s} \le t \le 6.696\ \text{s}) \\ 0 & (t > 6.696\ \text{s}) \end{cases} \tag{12}$$

3 Vehicle Vibration Simulation Using Matlab-Simulink Software

3.1 Input Parameters

The input parameters for simulating the differential equation system in Matlab-Simulink, based on the Toyota RAV4 and references [4, 6, 7, 9] are presented in Tab. 1.

Tab. 1 Parameters for simulating the system of vibration differential equations

Quantities	Values	Quantities	Values	Quantities	Values
V	8.33 m/s	m_{1R}	45 kg	C_{2L}	1 500 N·s/m
a_1	1.3 m	m_{2R}	45 kg	C_{1R}	1 500 N·s/m
a_2	1.5 m	m_{1L}	45 kg	C_{2R}	1 500 N·s/m
b_1	0.92 m	m_{2R}	45 kg	K_{1Lu}	220 000 N/m
b_2	0.94 m	K_a	1 200 N/m	K_{2Lu}	220 000 N/m
r_x	0.65 m	C_a	2 500 N·s/m	K_{1Ru}	220 000 N/m
r_y	0.3 m	K_{1L}	18 000 N/m	K_{2Ru}	220 000 N/m
J_x	600 kg·m^2	K_{2L}	18 000 N/m	C_{1Lu}	800 N·s/m
J_y	3 000 kg·m^2	K_{1R}	18 000 N/m	C_{2Lu}	800 N·s/m
m_a	100 kg	K_{2R}	18 000 N/m	C_{1Ru}	800 N·s/m
M	1 650 kg	C_{1L}	1 500 N·s/m	C_{2Ru}	800 N·s/m

3.2 Simulation Results

The simulation results in Matlab-Simulink for the rough road profiles are as follows:

- vibrations on a road with trapezoidal speed bumps (see Figs 5–10)

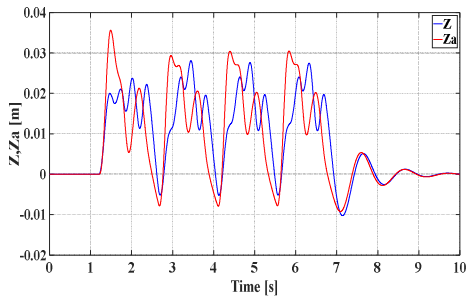

Fig. 5 Vertical displacements Z, Z_a

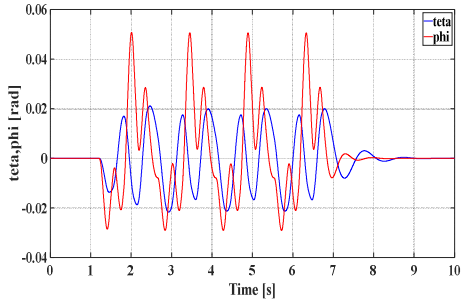

Fig. 6 Roll and pitch angular vibrations

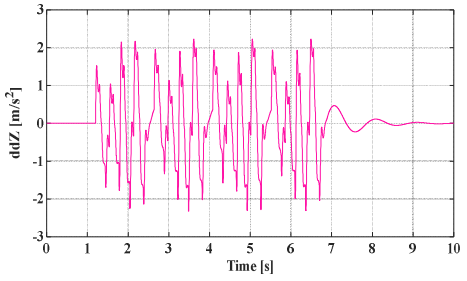

Fig. 7 Graph of vertical acceleration Z''

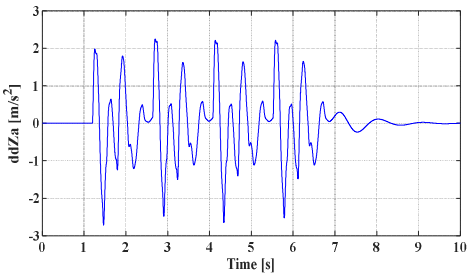

Fig. 8 Graph of vertical acceleration Z_a''

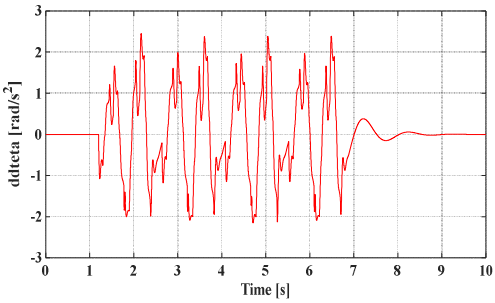

Fig. 9 Pitch angular acceleration

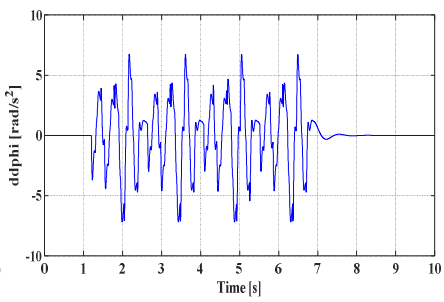

Fig. 10 Roll angular acceleration

- vibration on the semi-sinusoidal bumpy road surface (see Figs 11–16)

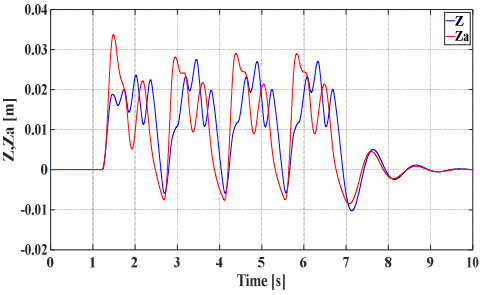

Fig. 11 Vertical displacements Z, Z_a

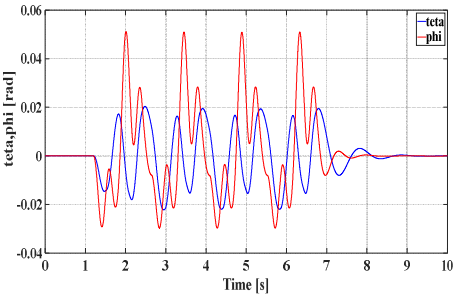

Fig. 12 Roll and pitch angular vibrations

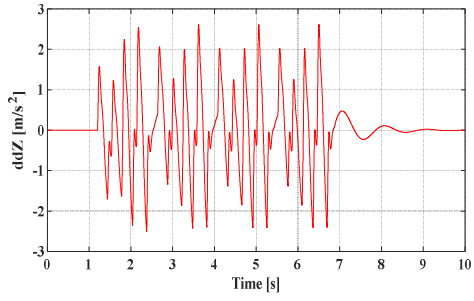

Fig. 13 Graph of vertical acceleration Z''

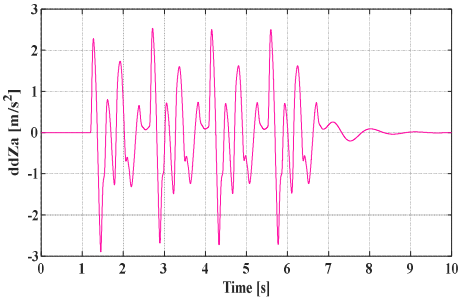

Fig. 14 Graph of vertical acceleration Z_a''

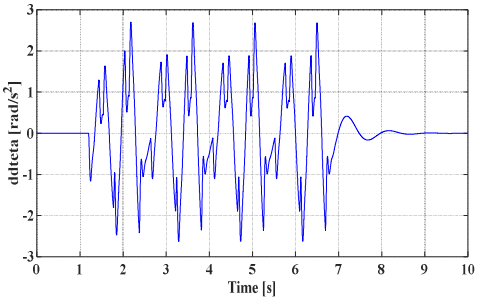

Fig. 15 Pitch angular acceleration

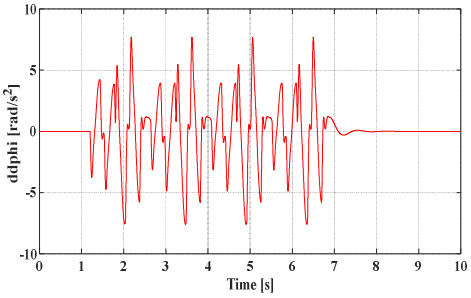

Fig. 16 Roll angular acceleration

- vibration on the rectangular bumby road surface (see Figs 17–22)

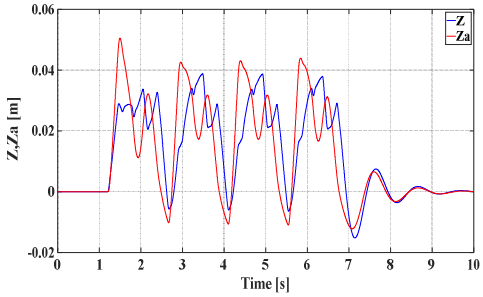

Fig. 17 Vertical displacements Z, Z_a

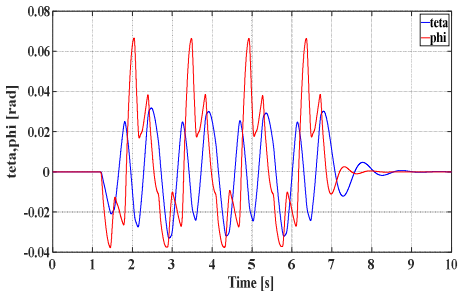

Fig. 18 Roll and pitch angular vibrations

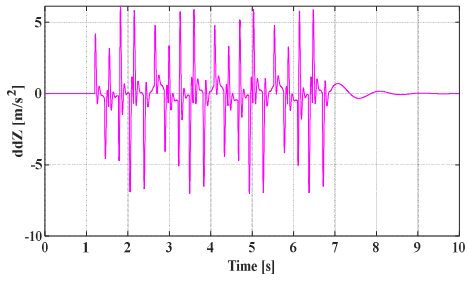

Fig. 19 Graph of vertical acceleration Z"

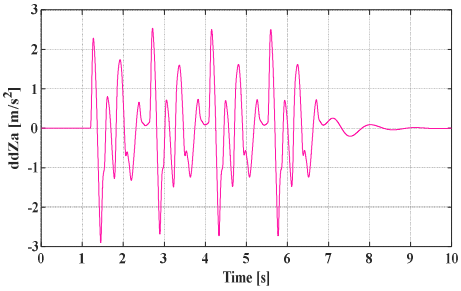

Fig. 20 Graph of vertical acceleration Z_a"

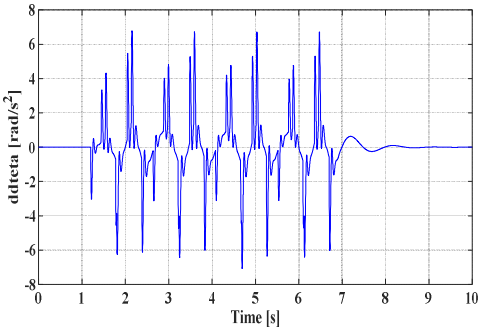

Fig. 21 Pitch angular acceleration

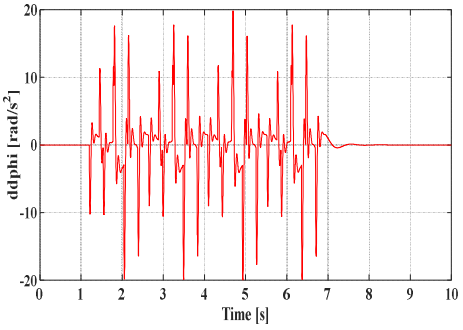

Fig. 22 Roll angular acceleration

The simulation results show that when the vehicle passes through four-speed bumps, the vertical and angular vibration graphs form four distinct vibration ranges, directly reflecting the sequential impact of each bump. The vertical vibration at the center of gravity of the vehicle (Figs 5, 11, 17) is simultaneously affected by the left and right road surface vibrations, so many small peaks appear alternating, showing the resonance of vibrations from both sides. At the driver's seat position (Figs 6, 12, 18), because this position is offset to the left, the influence of the left road surface is more obvious, creating higher vibration peaks than the impact from the right side. In particular, the vibration graph of the rectangular speed bump is zigzag, not as smooth and

less flat than the trapezoidal and semi-sine bumps, which reflect the abrupt and less smooth impact characteristics of this profile.

For pitch and roll angle vibrations, the simulation results show that pitch vibrations tend to be more stable and form four vibration ranges corresponding to the four-speed bumps arranged on both sides of the road. The vibration peak at the back is usually higher than at the front, due to the height of the right bump being larger than the left, resulting in a difference in impact. The roll angle vibrations with positive values tend to be larger than the negative values, reflecting the asymmetry in the distribution of dynamic loads. Although the vibration graphs of the three types of speed bumps have similar characteristics, the vibration value of the rectangular bump is always larger than that of the trapezoidal and semi-sine bumps. For the acceleration of the vibrations, the results show that the trapezoidal and semi-sine profiles give quite similar graphs, with relatively smooth and periodic changes. Meanwhile, the rectangular bump produces a significantly larger acceleration value, while the vibration changes continuously and is less flat, causing obvious discomfort and greatly affecting the smoothness of the vehicle.

4 Experimental Measurement of Vibrations on a Toyota RAV4 (2019)

The paper measured the vehicle's vibrations while passing over a single speed bump for both left and right wheels. The vehicle moved straight at a constant speed while passing over the speed bump [2]. The iDynamics software was used on a mobile device placed at the rear seat position. The recorded results were then analyzed using graphical representations. The test vehicle and the vibration measurement software interface are shown in Fig. 23.

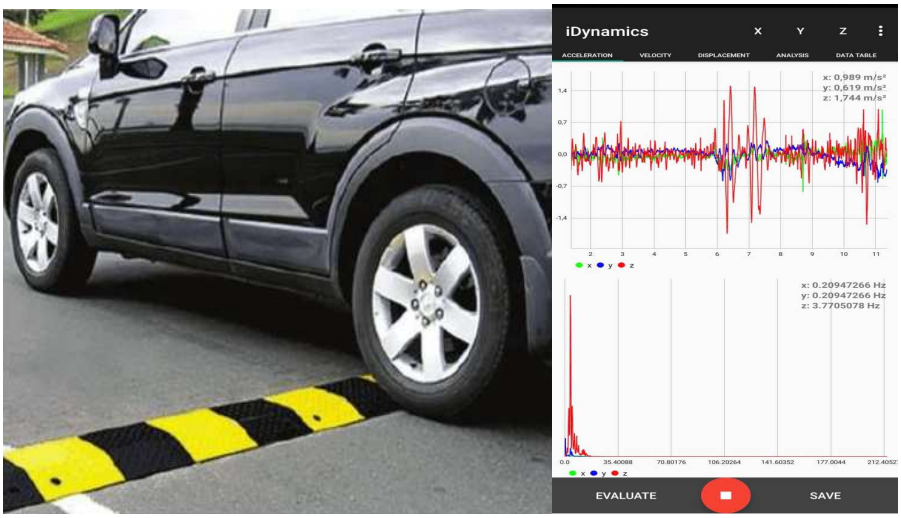

Fig. 23 Vehicle passing over a speed bump on the road with iDynamics vibration measurement software placed on the seat inside the vehicle

The study investigated two types of speed bumps: a semi-sine profile with a width of 30 cm and a height of 10 cm, and a trapezoidal profile with a width of 20 cm and a height of 15 cm. Their shapes are shown in Figs 24 and 25.

Fig. 24 Trapezoidal speed bump

Fig 25. Semi-sinusoidal speed bump

The obtained vibration measurement results are acceleration values in three directions x, y, z. For each vibration direction, the paper presents two types of graphs:

- graph of the entire process, showing the period from before the vehicle enters the speed bump to after it passes through,
- graph zooming in on the section where the vehicle passes over the speed bump, clarifying the change in acceleration values and the vibration response when the vehicle is affected by the bump.

The vehicle moves at an initial speed of v_0, the velocity at the top of the bump is v_{top}. When the vehicle climbs a bump of height h, a portion of kinetic energy is converted into potential energy:

$$\frac{1}{2}Mv_0^2 - Mgh = \frac{1}{2}Mv_{top}^2 \tag{13}$$

$$v_{top} = \sqrt{v_0^2 - 2gh} \tag{14}$$

The decrease in speed will be:

$$\Delta v = v_0 - v_{top} \tag{15}$$

The vehicle moved at an initial speed of 30 km/h for each test. A slight reduction in actual speed occurred when crossing the speed bump, with a variation of 0.65 km/h, which is acceptable for maintaining quasi-constant speed conditions during vibration measurement.

4.1 Vibration Measurement Results for the Trapezoidal Speed Bump

The vibration acceleration results along the *x*-axis of the vehicle are presented in Figs 26 and 27. The vibration acceleration along the *y*-axis is shown in Figs 28 and 29, while the vertical (*z*-axis) acceleration is illustrated in Figs 30 and 31.

The acceleration plots along the three axes (x, y, z) show that during the time interval from 0 to 9 s, the vibrations are small, corresponding to the flat road section before the vehicle reaches the speed bump. Between approximately 9.5 s and 11.5 s, the acceleration values spike sharply with high peaks, reflecting the strong impact as the vehicle passes over the speed bump. These peaks indicate that the acceleration reaches a maximum and then gradually decreases. After this interval, vibrations con-

tinue but with smaller amplitudes, indicating that the vehicle has passed the bump and returned to a stable state.

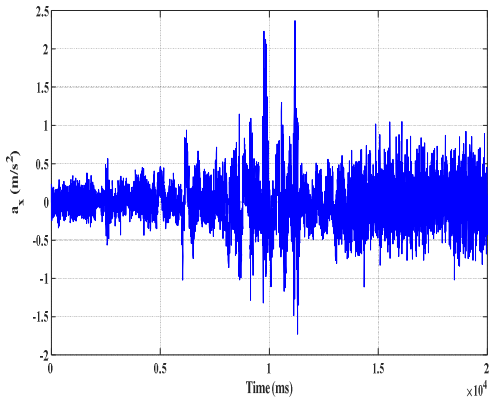

Fig. 26 Acceleration along the x-axis

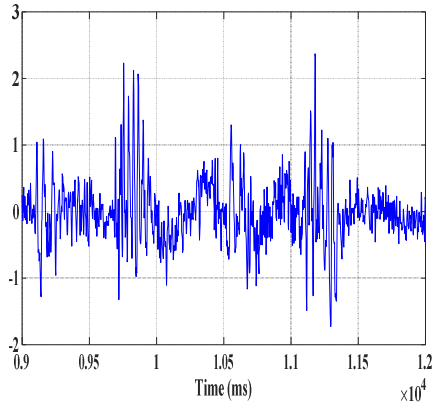

Fig. 27 Acceleration over the speed bump

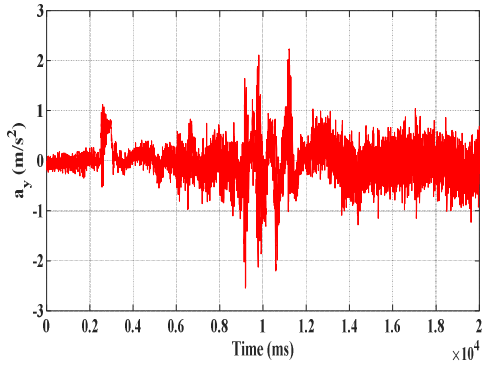

Fig. 28 Acceleration along the y-axis

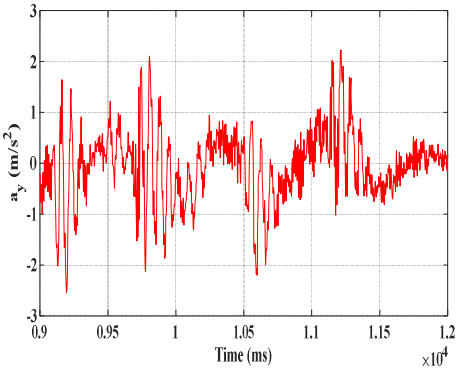

Fig. 29 Acceleration over the speed bump

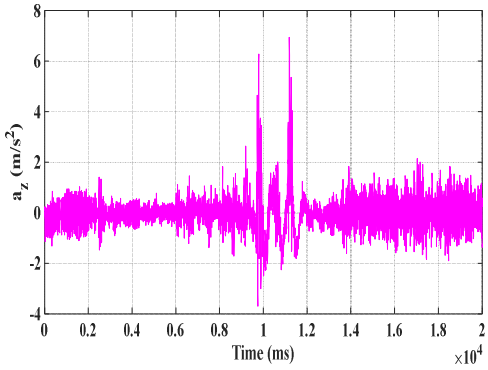

Fig. 30 Acceleration along the z-axis

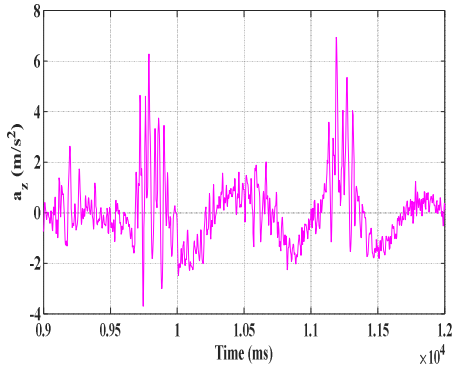

Fig. 31 Acceleration over the speed bump

When the vehicle passes over a trapezoidal speed bump, the vertical vibrations increase abruptly, with the largest amplitudes exceeding 7 m/s², significantly higher than those in the x and y directions. At the moment of direct contact with the bump, multiple sharp acceleration peaks occur consecutively, reflecting the strong impulse transmission from the road surface to the suspension and vehicle body. After passing the bump, the vibrations gradually diminish, but residual oscillations remain, indicating a prolonged effect on the vehicle's stability and ride comfort.

4.2 Vibration Measurement Results for the Semi-Sinusoidal Speed Bump

The vibration data obtained from the iDynamics software were analyzed and plotted in Figs 32–37. When the vehicle passed over bumps, strong vibrations were observed along all three axes (x, y, and z).

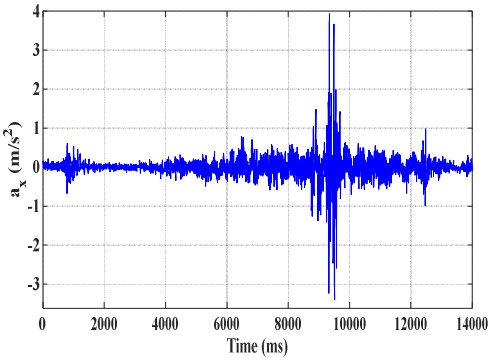

Fig. 32 Acceleration along the x-axis

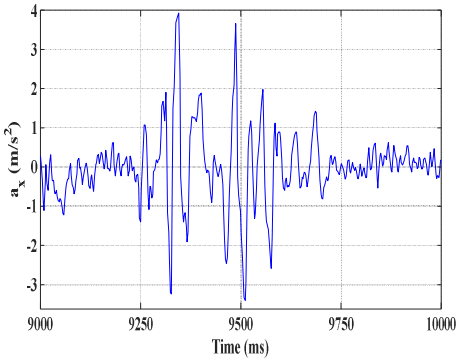

Fig. 33 Acceleration over the speed bump

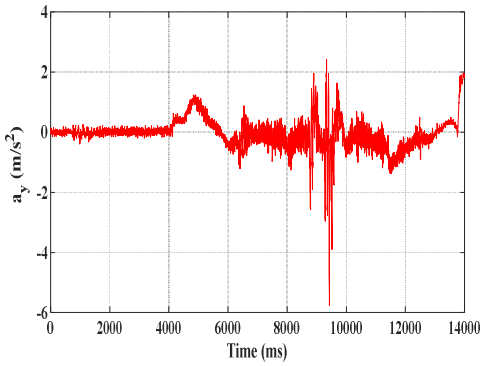

Fig. 34 Acceleration along the y-axis

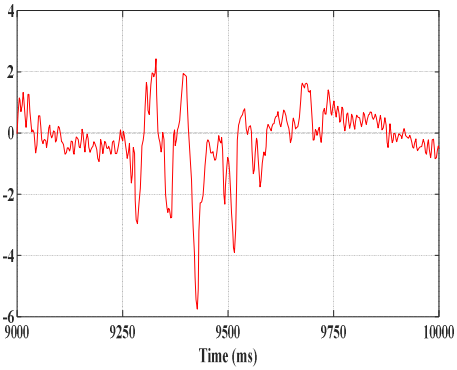

Fig. 35 Acceleration over the speed bump

The acceleration measurement results of the vehicle passing through the semi-sine speed bump show that the vibration acceleration of the car generally fluctuates slightly and is stable during the period when the car is moving on a flat road surface (from 0 to 9 s). When the car starts to pass through the speed bump (about 9 s to 10 s), the vibration amplitude increases sharply, with sharp peaks appearing in both positive and negative directions. After passing the bump (from 10 s onwards), the vibration gradually decreases and returns to a stable state. The acceleration amplitude value in

the vertical direction is much larger than in the other two directions. This shows that the speed bump causes a sudden change in the vertical vibration of the vehicle, causing a large acceleration that affects the suspension system and the occupants. These vibrations clearly reflect the impact effect of the wheel on the bump and are also the basis for evaluating the smoothness and working efficiency of the suspension system. The change in the width of the hump leads to a clear difference in the vibration range as well as the amplitude of the sudden vibration of the vehicle. In particular, when testing with a hump of greater height, the obtained vibration amplitude increases significantly, which is clearly demonstrated in all three vibration directions x, y, and z. This proves that the shape and size of the speed hump have a direct influence on the level of vibration and smoothness of the vehicle when moving over the speed hump, at the same time posing a requirement to consider the geometric factor of the hump reasonably in the design to balance the deceleration efficiency and driving comfort.

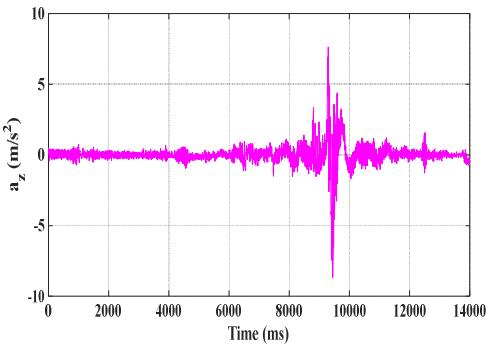

Fig. 36 Acceleration along the z-axis

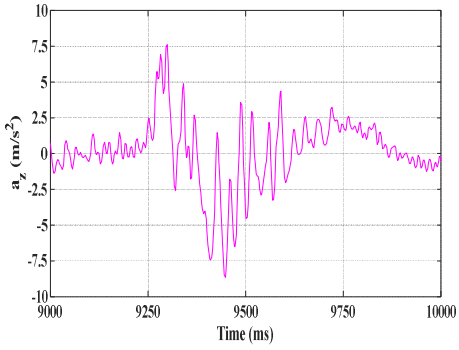

Fig. 37 Acceleration over the speed bump

5 Conclusion

Both the theoretical simulation and experimental results exhibit similar overall trends in the vibration responses of the vehicle when traversing speed bumps. In both cases, the vibration amplitudes increase sharply at the moment when the vehicle passes over the bumps, followed by a gradual decay as the suspension system dissipates the induced energy. The shapes of the acceleration-time histories are also consistent, confirming that the developed mathematical model accurately captures the essential dynamic characteristics of the vehicle-road interaction.

However, certain differences can be observed between the simulated and experimental results. In the experimental measurements, small irregular oscillations appear before and after the main impact peaks. These fluctuations are primarily caused by surface roughness and minor imperfections of the actual test track. In contrast, the simulation assumes an idealized smooth approach surface and perfectly defined bump geometry, resulting in smoother response curves.

The experimental results show that the measured accelerations include components along the longitudinal (x) and lateral (y) axes. This occurs because the vehicle's trajectory during motion is not perfectly straight. Even when traveling on a relatively flat road, small deviations in the driving direction cause the vehicle to oscillate slightly to the left or right, generating longitudinal and lateral accelerations. In addition, the presence of the driver or passengers introduces secondary vibrations (micro-motions)

due to body mass shifts during vehicle motion. As a result, the overall center of mass of the vehicle–occupant system is not completely fixed but exhibits slight oscillations along both the *x* and *y* directions. Moreover, the combined effects of the road surface and suspension system also contribute to these accelerations, since real road surfaces are never perfectly even. Small differences in surface roughness between the left and right or front and rear wheels generate pitch and roll motions, leading to additional vibrations in the longitudinal and lateral directions.

The results show that the shape and dimensions of speed bumps directly and significantly affect vertical vibrations, pitch, and roll of the vehicle body, thereby influencing ride comfort. Specifically, rectangular speed bumps with abrupt geometric profiles generate larger and more sudden acceleration variations compared to trapezoidal or semi-sinusoidal bumps, which have smoother geometric forms. Due to this characteristic, rectangular bumps produce higher vibration levels, reducing driver and passenger comfort, and potentially affecting the durability of the suspension system and tires. In contrast, semi-sinusoidal and trapezoidal bumps exhibit smoother vibration characteristics, with less abrupt acceleration changes, which is more favorable for ride comfort and reduces impact loads on the vehicle. Additionally, experimental results indicate that the width and height of speed bumps are key factors in determining vibration amplitude and frequency: taller and narrower bumps induce stronger vibrations, whereas wider bumps produce more distributed vibrations with fewer sudden shocks.

These analyses demonstrate that the shape and size of speed bumps not only influence vehicle speed control but also directly affect comfort and safety during operation. Therefore, the selection, design, and placement of speed bumps in practice should balance the goals of speed reduction with ride comfort and safety for road users. This study provides a useful scientific basis for the optimal design of speed bumps and opens avenues for further research on combining active suspension optimization to further enhance vehicle comfort and stability when passing over different types of speed bumps.

Acknowledgement

This work was created at the Department of Weapons and Ammunition, Faculty of Military Technologies, University of Defence. It was financed by the Ministry of Defence of the Czech Republic, project “Military autonomous and robotic assets” VAROPS (DZRO-FVT22-VAROPS).

References

[1] ZHIYONG, Y., R. ZHANG, Z. GUO, J. GUO and Y. ZHOU. Research on the Optimal Speed of Vehicles Passing Speed Bumps on the Highway Based on an Immune Algorithm. *Mechanical Sciences*, 2024, **15**(1), pp. 315-330. DOI 10.5194/ms-15-315-2024.

[2] KLIMENDA, F., J. SOUKUP, B. SKOČILASOVÁ and J. SKOČILAS. Vertical Vibration of the Vehicle when Crossing over Transverse Speed Bumps. *Manufacturing Technology Journal*, 2020, **20**(1), pp. 55-59. DOI 10.21062/mft.2020.020.

[3] UFUK, K. Vibration Levels Exposed at Speed Bump and Speed Hump Transitions. *Afyon Kocatepe University Journal of Science and Engineering*, 2022, **22**(2), pp. 332-341. DOI 10.35414/akufemubid.1031891.

[4] ZONGJUN, Y., R. SU and X. MA. Dynamic Responses of 8-DoF Vehicle with Active Suspension: Fuzzy-PID Control. *World Electric Vehicle Journal*, 2023, **14**(9), 249. DOI 10.3390/wevj14090249.

[5] CHEN, K., Z. MING and T. XUEFENG. Vibration Characteristic Analysis of Vehicle Air Suspension Based on Fuzzy Control. In: *Proceedings of the 2nd International Conference on Electronic & Mechanical Engineering and Information Technology (EMEIT 2012)*. Paris: Atlantis Press, 2022, pp. 2196-2199. DOI 10.2991/emeit.2012.486.

[6] BUI, V.D., M. MACKO, Z. KRYST, T.D. DUNG, D.Q. VI and P.H. NGUYEN. Mathematical Model of Unmanned Ground Vehicle. In: *International Conference QUAERE 2024* [online]. Hradec Kralove: Magnanimitas, 2024, pp. 765-771 [viewed 2025-08-27]. Available from: http://www.vedeckekonference.cz/library/proceedings/quaere_2024.pdf

[7] BUI, V.D., M. MACKO, T.D. DUNG, C. MARTIN and Z. KRYST. Research on Vibrations of an Unmanned Vehicle on a Random Road Surface. In: *2025 International Conference on Military Technologies (ICMT)*. Brno: IEEE, 2025. DOI 10.1109/ICMT65201.2025.11061271.

[8] KIM, Y.J., Y. SOHN, S. CHANG, S.B. CHOI and J.S. OH. Vibration Control of Car Body and Wheel Motions for In-Wheel Motor Vehicles Using Road Type Classification. *Actuators*, 2024, **13**(2), 80. DOI 10.3390/act13020080.

[9] ABDESELEM, B.B., M.D. MOMIR, S.D. ALEKSANDAR, R.P. SRETEN, G.B. ALEKSANDAR and B.F. ABDELLAH. Mathematical Modeling and Simulation of a Half-Vehicle Suspension System in the Roll Plane. *Military Technical Courier*, 2024, **72**(1), pp. 192-208. DOI 10.5937/vojtehg72-47551.